# On the Mechanism of Transfer of Sodium Ion across the Nitrobenzene/Water Interface Facilitated by Dibenzo-18-crown-6

Tadaaki KAKUTANI, Yoshinori NISHIWAKI,† Toshiyuki OSAKAI,† and Mitsugi SENDA*,†
Research Center for Cell and Tissue Culture, Faculty of Agriculture, Kyoto University, Kyoto 606
†Department of Agricultural Chemistry, Faculty of Agriculture, Kyoto University, Kyoto 606
(Received November 1, 1985)

The question of the site of ionophore–ion complex formation, whether it is in the organic phase (EC), in the aqueous phase (CE), or at the interface (E), in the transfer facilitated by dibenzo-18-crown-6 of sodium ion across the nitrobenzene/water interface was studied by kinetic analysis of the ion transfer using a.c. polarographic method. The results indicate that the interface reaction mechanism (E) is the most probable of the three.

The transfer of alkali metal and alkaline earth metal ions across the organic solvent or oil(O)/water(W) interface facilitated by the presence of natural or synthetic ionophores, such as valinomycin, nonactin, and crown ethers in the organic phase, has been intensively studied by Koryta[1] and his group,[2–9] Wang and Pang[10] and Yoshida and Freiser[11] using various electrochemical techniques. Despite the great effort devoted to elucidate the mechanism of the ionophore-mediated ion transport, the central question about the site of the complex formation and its dissociation, whether it is in the organic phase (EC mechanism), in the aqueous phase (CE mechanism) or at the interface (E mechanism), has not been settled yet. Koryta et al.[6] came to the conclusion that the valinomycin-facilitated transfer of potassium ion across the nitrobenzene/water interface takes place via two mechanisms, the EC and E mechanisms in parallel. Experimental results suggesting the interface reaction mechanism (E mechanism) have also been presented.[12] By contrast, Yoshida and Freiser[11] have presented experimental evidence which they interpret as meaning that potassium ion reacts in the aqueous phase with valinomycin that has transferred from the nitrobenzene phase (that is, CE mechanism). Quite recently, Lin and Freiser[24] have presented further experimental results suggesting that the mechanism of the potassium ion transfer facilitated by dibenzo-18-crown-6 across the 1,2-dichloroethane/water interface may depend on the concentration of potassium ion in the aqueous phase. The facilitated transfer of the alkali metal ions at the O/W interface is a very rapid process and is diffusion-controlled when observed using electrochemical methods such as cyclic voltammetry,[1–9,12] chronopotentiometry,[10] and current-scan polarography with an electrolyte dropping electrode.[11] In our opinion, the answer about the mechanism can be obtained only by kinetic study of the formation and dissociation of the ion-ionophore complex at and near the interface.

In previous papers,[13,14] we have shown that the a.c. polarographic method is useful in studying the kinetics and mechanism of ion transfer across the O/W interface. In this study[15] we have applied the a.c. polarographic method to study the facilitated transfer of sodium ion across the nitrobenzene/water interface in the presence of dibenzo-18-crown-6 (DB18C6) in the nitrobenzene phase and attempted to elucidate its mechanism on the basis of the analysis of kinetic parameters obtained by this method.

## Experimental

**Chemicals.** Tetrapentylammonium chloride (TPACl) and tetramethylammonium chloride (TMACl) were obtained commercially. Triply distilled water was used to prepare the aqueous electrolyte solution. An aqueous solution of TPACl was stirred with silver chloride overnight and the filtrate was used. The concentrations of TPACl and TMACl were determined by potentiometric titration with a standard silver nitrate solution. Tetrapentylammonium tetraphenylborate (TPATPB) was prepared by the equimolar addition of an ethanol solution of tetrapentylammonium iodide to an ethanol solution of sodium tetraphenylborate. The resulting precipitate was repeatedly washed with twice-distilled water and recrystallized several times from an ethanol–acetone (3:2) mixture. Commercial DB18C6 was twice recrystallized from benzene and was dried at 80 °C under reduced pressure. Analytical-grade nitrobenzene was purified by a method previously described.[13] The nitrobenzene solution of TPATPB was prepared in the dark just before use. The other chemicals of commercial analytical grade were used as received.

**Electrochemical Measurements.** The electrolytic cell used here was essentially the same as that described elsewhere.[13] A flat test interface with an area of 0.241 $cm^2$ was formed at the end of a glass tube, which was treated in advance with dimethyldichlorosilane as described before.[16] The test interface was renewed for each measurement of a single voltammogram or a single chronoamperometric current-time curve.

The electrochemical cell was:

I

(RE1) Ag | AgCl | 0.1 mol dm$^{-3}$ $MgSO_4$ + 0.02 mol dm$^{-3}$ TPACl (W)

II

| 0.1 mol dm$^{-3}$ TPATPB + (0—2) × 10$^{-3}$ mol dm$^{-3}$ DB18C6 (NB)

* III

| 0.05—0.2 mol dm$^{-3}$ NaCl (W)

| AgCl | Ag (RE2) Cell I

The O/W interface to be investigated is marked by*. The reference electrode for the nitrobenzene phase, RE1, was a Ag/AgCl/0.1 mol dm$^{-3}$ $MgSO_4$, 0.02 mol dm$^{-3}$ TPACl(W) electrode that was connected to nitrobenzene phase II through sintered glass. The reference electrode for the aqueous phase, RE2, was a Ag/AgCl electrode and was directly immersed in aqueous phase III. The surface areas of these two Ag/AgCl electrodes were greater than 4 cm$^2$. This reference electrode system was stable and gave reproducible results.

All voltammetric measurements were done at 25±0.1 °C with a two-electrode cell system.[13] In a.c. polarographic measurements, a.c. voltage of small amplitude (usually 5 mV peak to peak) was superimposed on the linear sweep voltage scanned usually at the rate of 5 mV s$^{-1}$. The a.c. frequency range was between 10 and 100 Hz. Other details concerning apparatus and procedures of electrochemical measurements were described elsewhere.[13]

## Results

The potential applied to Cell I, $E$, was defined as the potential of the terminal of RE2, $E_{RE2}$, against that of RE1, $E_{RE1}$, that is, $E=E_{RE2}-E_{RE1}$. The flow of positive charge from the aqueous solution (phase III) to the nitrobenzene solution (phase II) was taken to be the positive current. Electrochemical measurements were done under conditions in which the bulk concentration of $Na^+$ ion in the aqueous phase, $^*C_M^W$, was much higher than that of DB18C6 in the nitrobenzene phase, $^*C_L^O$; $(^*C_M^W/^*C_L^O)\geq 50$ in cyclic voltammetry and chronoamperometry and $(^*C_M^W/^*C_L^O)\geq 100$ in a.c. polarography.

**Cyclic Voltammetry and Potential-Step Chronoamperometry.** Figure 1 shows cyclic voltammograms for the transfer of $Na^+$ ion across the interface between a 0.1 mol dm$^{-3}$ NaCl aqueous solution and a 0.1 mol dm$^{-3}$ TPATPB nitrobenzene solution in the presence (curve a) and absence (curve b) of DB18C6 in the nitrobenzene phase. When DB18C6 was present in the nitrobenzene phase, a cyclic voltammogram due to the facilitated transfer of $Na^+$ ion was observed. The positive and negative peak currents, $I_{pa}$ and $I_{pc}$, when corrected for the base current, were

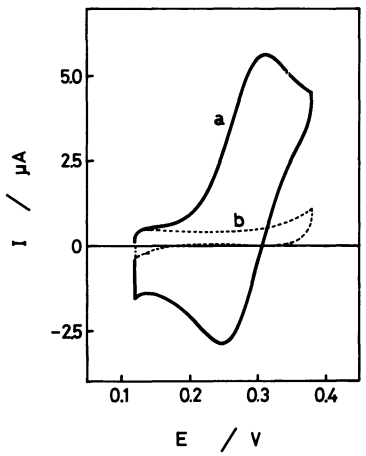


Fig. 1. Cyclic voltammograms of $Na^+$-ion transfer across the interface between a 0.1 mol dm$^{-3}$ NaCl aqueous solution and a 0.1 mol TPATPB nitrobenzene solution in the presence (a) and the absence (b) of 0.5 × 10$^{-3}$ mol dm$^{-3}$ DB18C6 in the nitrobenzene phase.

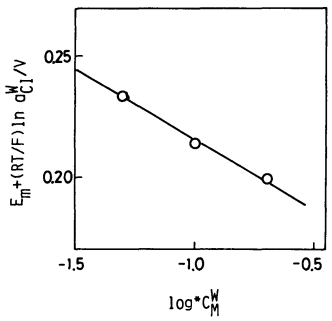


Fig. 2. Plot of $E_m+(RT/F)\ln a_{Cl}^W$ against $\log {}^*C_M^W$.

proportional to $^*C_L^O$ between 0.5 and 2×10$^{-3}$ mol dm$^{-3}$ and also to the square root of the voltage scan rate, $v$, in the range of 5 to 50 mV s$^{-1}$, whereas they were independent of $^*C_M^W$ between 0.05 and 0.2 mol dm$^{-3}$. These results indicate that the current is controlled by diffusion of DB18C6 toward the interface. The positive and negative peak potentials, $E_{pa}$ and $E_{pc}$, and the midpoint potential, $E_m$, defined by $E_m=(E_{pa}+E_{pc})/2$, were independent of both $^*C_L^O$ and $v$. The peak-separation, $\Delta E_p$, defined by $\Delta E_p=E_{pa}-E_{pc}$, was 65±5 mV over the ranges studied of $^*C_L^O$ and $v$. On the other hand, an increase in $^*C_M^W$ caused a negative shift in $E_m$ (or in $E_{pa}$ and $E_{pc}$), when corrected for the potential change of RE2 due to the change of the $Cl^-$ concentration in the aqueous phase, $^*C_{Cl}^W(=^*C_M^W)$. That is, a plot of the corrected midpoint potential, $(E_m)_{corr}=E_m+(RT/F)\ln a_{Cl}^W$, $a_{Cl}^W$ being the activity of $Cl^-$ ion in the aqueous phase III, against $\log {}^*C_M^W$ yielded a straight line with a slope of −59 mV (Fig. 2).

In potential-step chronoamperometry[16] the currents were measured at the time $t$=10 s after

application of the potential step $E$ and being corrected for the base current. The plot of the current, $I_{t=10\,s}$, against $E$ gave well-defined current-potential curves, as shown in Fig. 3. The limiting current, $(I_{t=10\,s})_l$, was proportional to $^*C_L^o$. A plot of $E$ against $\log\{(I_{t=10\,s})/[(I_{t=10\,s})_l-(I_{t=10\,s})]\}$ yielded a straight line with the slope of 58±2 mV over the $^*C_L^o$ range studied. The half-wave potential, $E_{1/2}$, coincided with the $E_m$ of the corresponding cyclic voltammogram.

**A.c. Polarography.** In Fig. 4, curves a and a′ show the real ($Y_t'$) and imaginary ($Y_t''$) components of the admittance plotted against the linear sweep voltage, that is, the applied d.c. potential, $E_{d.c.}$, for the transfer of $Na^+$ ion across the interface between a 0.1 mol dm$^{-3}$ NaCl aqueous solution and a 0.1 mol dm$^{-3}$ TPATPB nitrobenzene solution containing $0.5\times10^{-3}$ mol dm$^{-3}$ DB18C6. After correction for the base admittance (curves b and b′), these admittances give the real ($Y_F'$) and imaginary ($Y_F''$) components of the facilitated transfer of $Na^+$ ion at the nitrobenzene/water interface. The summit potentials of the $Y_F'$ vs. $E_{d.c.}$ and $Y_F''$ vs. $E_{d.c.}$ curves agreed well within experimental error with each other and with the midpoint potential of the corresponding cyclic voltammogram (Fig. 1). The ion-transfer admittance can be expressed by a series combination of an equivalent resistance, $r_s$, and an equivalent capacitance, $c_s$.[13] Figure 5 shows the plots of $r_s$ and $1/\omega c_s$ at $E_{d.c.}=E_{1/2}=0.275$ V against $\omega^{-1/2}$ ($\omega=2\pi f$, $f$ being the a.c. frequency) of the ion transfer across the same interface as that in curves a and a′ in Fig. 4. Both plots gave straight lines with a common slope. Similar linear plots of $r_s$ and $1/\omega c_s$, each set with a common slope, $\sigma$, were obtained at several other d.c.

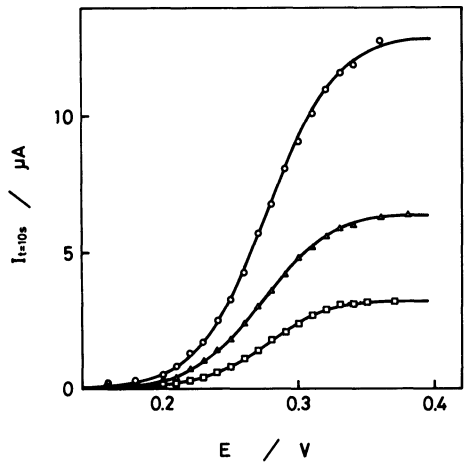


Fig. 3. Plot of $I_{t=10\,s}$, corrected for the base current, against $E$ for the $Na^+$-ion transfer across the interface between a 0.1 mol dm$^{-3}$ NaCl aqueous solution and a 0.1 mol dm$^{-3}$ TPATPB nitrobenzene solution containing $0.5\times10^{-3}$ (□), $1.0\times10^{-3}$ (△), and $2.0\times10^{-3}$ (○) mol dm$^{-3}$ DB18C6.

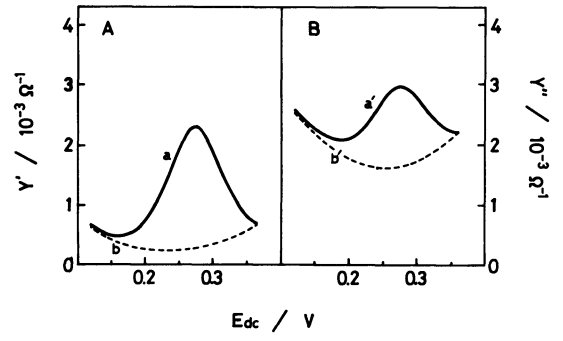


Fig. 4. Real (A) and imaginary (B) components of the admittance of the interface between a 0.1 mol dm$^{-3}$ NaCl aqueous solution and a 0.1 mol dm$^{-3}$ TPATPB nitrobenzene sotution, at $f=50$ Hz, in the presence (a and a′) and the absence (b and b′) of $0.5\times10^{-3}$ mol dm$^{-3}$ DB18C6 in the nitrobenzene phase.

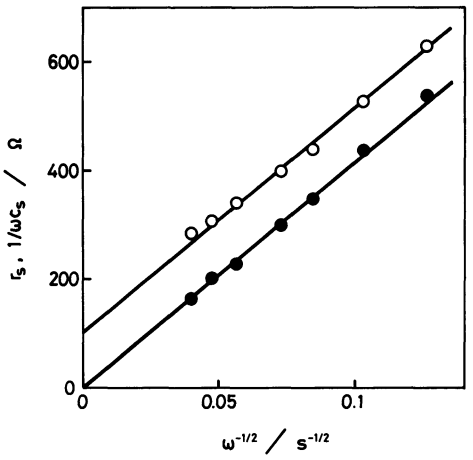


Fig. 5. Plots of the real (○) and imaginary (●) components of the ion transfer impedance at $E_{d.c.}=E_{1/2}^r=0.275$ V against $\omega^{-1/2}$, for the $Na^+$-ion transfer across the interface between a 0.1 mol dm$^{-3}$ NaCl aqueous solution and a 0.1 mol dm$^{-3}$ TPATPB nitrobenzene solution containing $0.5\times10^{-3}$ mol dm$^{-3}$ DB18C6.

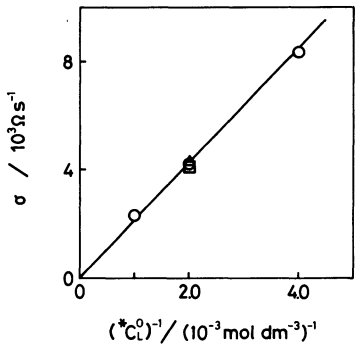


Fig. 6. Plot of $\sigma$ at $E_{d.c.}=E_{1/2}^r$ against $(^*C_L^o)^{-1}$. $^*C_M^w$: (△) 0.05, (○) 0.1, and (□) 0.2 mol dm$^{-3}$.

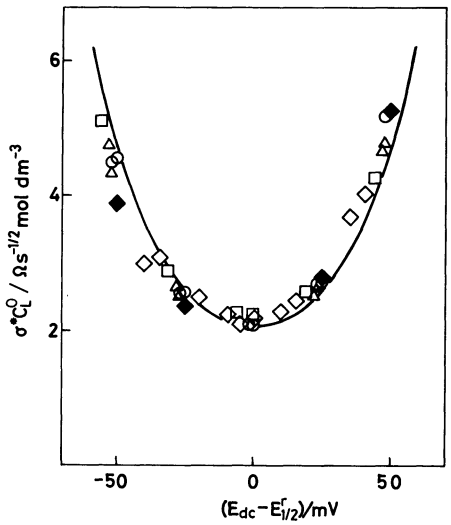


Fig. 7. Plot of $\sigma^*C_L^o$ against $(E_{d.c.}-E_{1/2}^r)$.
(○): $^*C_L^o=0.25\times10^{-3}$ and $^*C_M^w=0.1$ mol dm$^{-3}$, (△): $^*C_L^o=0.5\times10^{-3}$ mol dm$^{-3}$ and $^*C_M^w=0.1$ mol dm$^{-3}$, (□): $^*C_L^o=1\times10^{-3}$ mol dm$^{-3}$, and $^*C_M^w=0.1$ mol dm$^{-3}$, (◇): $^*C_L^o=0.5\times10^{-3}$ mol dm$^{-3}$ and $^*C_M^w=0.05$ mol dm$^{-3}$, (◆): $^*C_L^o=0.5\times10^{-3}$ mol dm$^{-3}$ and $^*C_M^w=0.2$ mol dm$^{-3}$.
The solid line is the theoretical one drawn by Eq. 22 with $D_L^o=2.3\times10^{-6}$ cm$^2$ s$^{-1}$.

potentials in the range of $|E_{d.c.}-E_{1/2}|\leq0.05$ V for the interface between an aqueous solution of 0.05—0.2 mol dm$^{-3}$ NaCl and a nitrobenzene solution of 2.5×10$^{-4}$—1×10$^{-3}$ mol dm$^{-3}$ DB18C6 containing 0.1 mol dm$^{-3}$ TPATPB. Figure 6 shows a plot of $\sigma$ obtained at $E_{d.c.}=E_{1/2}$ against $1/^*C_L^o$, indicating that $\sigma$ was inversely proportional to $^*C_L^o$ but independent of $^*C_M^w$. The same dependence of $\sigma$ on $^*C_L^o$ was observed at other $E_{d.c.}$'s at $|E_{d.c.}-E_{1/2}|\leq0.05$ V. Also, the $\sigma$ values changed with $E_{d.c.}-E_{1/2}$ for a given set of $^*C_L^o$ and $^*C_M^w$ (see Fig. 7 below).

## Discussion

When in the organic phase there is a lipophilic ligand, L, (usually belonging to the family of ionophores) that forms a lipophilic complex $ML_n$ ($n$=1,2,...) with the transferring ion $M^z$ ($z$=the number of charges), the transfer of $M^z$ ion from the aqueous to the organic phase is facilitated; that is, it takes place at a less positive (if $z>0$) or at a less negative (if $z<0$) potential of the aqueous phase referred to that of the organic phase.[12] From a kinetic viewpoint, three kinds of the mechanisms of facilitated ion transfer may be postulated. In the following, we assume that the lipophilic ligand L is a neutral carrier.

**(1) EC Mechanism.** The ion $M^z$ is transferred from the W to the O phase (Eq. 1a), followed by the formation of a complex $ML_n$ with the ligand L (Eq. 1b) in the O phase:

$$M^z(W) \underset{\vec{k}_{M(E)}}{\overset{\vec{k}_{M(E)}}{\rightleftharpoons}} M^z(O), \tag{1a}$$

$$M^z(O) + nL(O) \underset{k_1^b}{\overset{k_1^f}{\rightleftharpoons}} ML_n^z(O) \quad K^o = k_1^f/k_1^b. \tag{1b}$$

**(2) CE Mechanism.** The ligand L is first transferred from the O to the W phase (Eq. 2a) and forms the complex $ML_n$ with the ion $M^z$ in the W phase (Eq. 2b); this is followed by the transfer of the complex from the W to the O phase (Eq. 2c):

$$L(O) \underset{k_L^b}{\overset{k_L^f}{\rightleftharpoons}} L(W) \qquad d_L = k_L^b/k_L^f, \tag{2a}$$

$$M^z(W) + nL(W) \underset{k_2^b}{\overset{k_2^f}{\rightleftharpoons}} ML_n^z(W) \quad K^w = k_2^f/k_2^b, \tag{2b}$$

$$ML_n^z(W) \underset{\vec{k}_{ML(E)}}{\overset{\vec{k}_{ML(E)}}{\rightleftharpoons}} ML_n^z(O). \tag{2c}$$

**(3) E Mechanism.** The complex $ML_n$ is formed in a single step taking place at the O/W interface:

$$M^z(W) + nL(O) \underset{\vec{k}_{M/ML(E)}}{\overset{\vec{k}_{M/ML(E)}}{\rightleftharpoons}} ML_n^z(O). \tag{3}$$

Differential equations to express the diffusion coupled with complex formation of M, L, and $ML_n$ in both organic and aqueous phases can easily be written and were solved, under appropriate conditions and assumptions, to give the theoretical equations of the polarographic (normal pulse polarographic) current-potential curves and also of the a.c. impedance of the ion transfer for each of these three mechanisms. Detailed results will be published elsewhere. Here only those important results relevant to discussion of the mechanism will be given.

Let us first assume (1) that the bulk concentration of $M^z$ ion in the aqueous phase, $^*C_M^w$, is exceedingly large compared with that of L in the organic phase, $^*C_M^w \gg {}^*C_L^o$ (see Results), (2) that the partition coefficient of the carrier between the organic and aqueous phases, $d_L=C_L^o/C_L^w$, is so large ($d_L \gg 1$) that the presence of L in the bulk of the aqueous phase can be neglected, and (3) that the complex formation in the organic phase is largely shifted to the complex side ($K^oC_M^o \gg 1$) so that the presence of $M^z$ ion in the organic phase can virtually be neglected. Then the reversible (*Nernstian*) normal pulse polarographic wave ($I$–$E$ curve) of facilitated ion transfer can be expressed for the three mechanisms by the same equation:

$$E = E_M^\ominus - (RT/zF)\ln K^o - (RT/zF)\ln {}^*C_M^w + (RT/zF)\ln[(\kappa_L^o)^n/\kappa_{ML}^o] + (RT/zF)\ln[I/(I_1-I)^n], \tag{4}$$

with

$$\kappa_L^\circ = (D_L^\circ/n^2\pi t)^{1/2} \quad \text{and} \quad \kappa_{ML}^\circ = (D_{ML}^\circ/\pi t)^{1/2} \tag{5}$$

where $E_M^\circ$ is the standard ion transfer potential of Eq. 1a with respect to the reference electrode system (see Eq. 11 below) of Cell I and is related to the standard ion-transfer potentials of Eqs. 2c and 3, $E_{ML}^\circ$ and $E_{M/ML}^\circ$, respectively, both with respect to the same reference electrode system as above, by

$$E_M^\circ - (RT/zF)\ln K^\circ = E_{ML}^\circ - (RT/zF)\ln K^w + (RT/zF)\ln (d_L)^n \tag{6}$$

$$= E_{M/ML}^\circ. \tag{7}$$

In these equations $K^\circ$ ($=k_1^f/k_1^b$) and $K^w$ ($=k_2^f/k_2^b$) are the formation constants of Eqs. 1b and 2b, $D_L^\circ$ and $D_{ML}^\circ$ are the diffusion coefficients of L and $ML_n$ in the organic phase, respectively, $t$ is time measured from the voltage pulse rise, and $I_l$ is the limiting diffusion current given by

$$I_l = zFA{*C_L^\circ}(D_L^\circ/n^2\pi t)^{1/2}, \tag{8}$$

where $A$ is the electrode surface area, and $F$, $R$, and $T$ are used in their usual meanings.

Experimental results by cyclic voltammetry and potential-step chronoamperometry (normal pulse polarography) all indicate that the $Na^+$ ion transfer facilitated by DB18C6 at the nitrobenzene/water interface is d.c. reversible (*Nernstian*). That $E_m$ and $E_{1/2}$ coincide with each other and are independent of ${*C_L^\circ}$, and also that the log $[I/(I_l-I)]$ vs. $E$ plot is linear with the reciprocal slope of 58±2 mV both indicate that $n$=1, that is, that there is formation of a 1:1 complex. Then Eq. 4 can be rewritten as Eq. 9 with the reversible half-wave potential $E_{1/2}^r$ defined by Eq. 10:

$$E = E_{1/2}^r + (RT/zF)\ln [I/(I_l-I)], \tag{9}$$

$$E_{1/2}^r = E_M^\circ + (RT/2zF)\ln (D_L^\circ/D_{ML}^\circ) - (RT/zF)\ln K^\circ - (RT/zF)\ln {*C_M^w}. \tag{10}$$

The observed dependence of $E_{1/2}(=E_m)$ on log ${*C_M^w}$ (Fig. 2) was explained well by Eq. 10.

The potential $E$ is usually expressed by

$$E = \Delta\phi + \Delta E_{ref}, \tag{11}$$

where $\Delta\phi$ is the potential difference between phases II and III in Cell I and $\Delta E_{ref}$ is the constant determined by the reference electrode system in Cell I, that is, RE1 and RE2 (see Experimental). In Cell I with 0.1 mol $dm^{-3}$ TPATPB (NB, phase II)/0.1 mol $dm^{-3}$ NaCl (W, phase III), $\Delta E_{ref}$ was determined to be 0.275 V from the reversible half-wave potential of tetramethylammonium ($TMA^+$) ion measured with the same reference electrode system as that used here and $\Delta\phi_{TMA}^\circ$=0.035 V.[17] Then, $E_M^\circ=E_{Na}^\circ$ ($=\Delta\phi_{Na}^\circ+\Delta E_{ref}$) was calculated to be 0.629 V using $\Delta\phi_{Na}^\circ$=0.354 V.[17] Finally log $K^\circ$ was calculated to be 7.0 by Eq. 10 by assuming $D_L^\circ=D_{ML}^\circ$. Also, using the values from the literatures of $d_L=2.3\times10^4$ [18] and $K^w$=14.6 $mol^{-1}$ $dm^3$,[19] $E_{ML}^\circ$ ($=\Delta\phi_{ML}^\circ+\Delta E_{ref}$) was calculated by Eq. 6 (with $n$=1) to be 0.028 V, which gives $\Delta\phi_{ML}^\circ$=−0.248 V. Similarly, $E_{M/ML}^\circ$ was calculated by Eq. 7 to be 0.216 V, which gives $\Delta\phi_{M/ML}^\circ$=−0.059 V.

In addition to the above assumptions (1)—(3), we further assume that the facilitated ion transfer processes are d.c. reversible. Then $r_s$ and $1/\omega c_s$ of the facilitated ion transfer by 1:1 complex formation can be written[20] for each of the above three mechanisms, while assuming that $D_L^\circ=D_{ML}^\circ$, as follows.

**(1) EC Mechanism:**

$$r_s = \frac{RT}{z^2F^2A}\left[\frac{1}{\vec{k}_M(E_{d.c.}){*C_M^w}} + \frac{K^\circ}{\rho_c}\cdot\left(\frac{1+\rho_c}{k_1^f D_L^\circ {*C_L^\circ}}\right)^{1/2}\right] + \frac{RT}{z^2F^2A}\cdot\frac{1}{{*C_L^\circ}\sqrt{2\omega D_L^\circ}}\cdot\frac{(1+\rho_c)^2}{\rho_c}, \tag{12}$$

$$1/\omega c_s = \frac{RT}{z^2F^2A}\cdot\frac{1}{{*C_L^\circ}\sqrt{2\omega D_L^\circ}}\cdot\frac{(1+\rho_c)^2}{\rho_c}, \tag{13}$$

and

$$r_k \equiv (r_s - 1/\omega c_s) = \frac{RT}{z^2F^2A}\left[\frac{1}{\vec{k}_M(E_{d.c.}){*C_M^w}} + \frac{K^\circ}{\rho_c}\left(\frac{1+\rho_c}{k_1^f D_L^\circ {*C_L^\circ}}\right)^{1/2}\right] \tag{14}$$

with

$$\rho_c = \exp[zF(E_{d.c.} - E_{1/2}^r)/RT] \tag{15}$$

Here it is also assumed that the equilibrium and rate constants of the complex formation reaction in the organic plhase, $K^\circ$ and $k_1^f$, are so large that the conditions $K^\circ{*C_L^\circ} \gg (\rho_c+1)^2$ and

$$\frac{k_1^f}{\omega}\left[\frac{K^\circ{*C_L^\circ}+(1+\rho_c)^2}{K^\circ(1+\rho_c)}\right] \gg \left[\frac{K^\circ{*C_L^\circ}}{\sqrt{2}(1+\rho_c)^2}\right]^{2/3}$$

are simultaneously satisfied.

**(2) CE Mechanism:**

$$r_s = \frac{RT}{z^2F^2A}\cdot\frac{(1+\rho_c)d_L}{K^w{*C_M^w}{*C_L^\circ}}\times\left[\frac{1}{\vec{k}_{ML}(E_{d.c.})} + \left(\frac{K^w(K^w{*C_M^w}+1)}{k_2^f D^w}\right)^{1/2}\right] + \frac{RT}{z^2F^2A}\cdot\frac{1}{{*C_L^\circ}\sqrt{2\omega D_L^\circ}}\cdot\frac{(1+\rho_c)^2}{\rho_c} \tag{16}$$

$$1/\omega c_s = \frac{RT}{z^2F^2A}\cdot\frac{1}{{*C_L^\circ}\sqrt{2\omega D_L^\circ}}\cdot\frac{(1+\rho_c)^2}{\rho_c} \tag{17}$$

and

$$r_k \equiv (r_s - 1/\omega c_s) = \frac{RT}{z^2F^2A}\cdot\frac{(1+\rho_c)d_L}{K^w{*C_M^w}{*C_L^\circ}}\times\left[\frac{1}{\vec{k}_{ML}(E_{d.c.})} + \left(\frac{K^w(K^w{*C_M^w}+1)}{k_2^f D^w}\right)^{1/2}\right]. \tag{18}$$

In Eqs. 16—18 the following three conditions are also assumed: (a) the rate constant of the transfer of L across the interface is large enough to satisfy $2k_L^f/\sqrt{2\omega D_L^\circ} \gg 1$, (b) the partition coefficient is large enough to satisfy both $d_L \gg (D^w/D_L^\circ)^{1/2}$ and $[(D^w/D_L^\circ)^{1/2}+d_L]/K^w{}^*C_M^w \gg 1$ (where $D^w$ is the common diffusion coefficient in the aqueous phase; $D^w=D_M^w=D_L^w=D_{ML}^w$), and (c) the rate constant of the complex formation in the aqueous phase is very large enough to satisfy $\xi=k_2^f(K^w{}^*C_M^w+1)/\omega K^w \gg 1$ and $\xi \gg 2(K^w{}^*C_M^w)^2$ simultaneously.

**(3) E Mechanism:**

$$r_s = \frac{RT}{z^2F^2A}\cdot\frac{(1+\rho_c)}{\vec{k}_{M/ML}(E_{d.c.})^*C_M^w{}^*C_L^\circ} + \frac{RT}{z^2F^2A}\cdot\frac{1}{^*C_L^\circ\sqrt{2\omega D_L^\circ}}\cdot\frac{(1+\rho_c)^2}{\rho_c}, \quad (19)$$

$$1/\omega c_s = \frac{RT}{z^2F^2A}\cdot\frac{1}{^*C_L^\circ\sqrt{2\omega D_L^\circ}}\cdot\frac{(1+\rho_c)^2}{\rho_c}, \quad (20)$$

and

$$r_k \equiv (r_s - 1/\omega c_s) = \frac{RT}{z^2F^2A}\cdot\frac{(1+\rho_c)}{\vec{k}_{M/ML}(E_{d.c.})^*C_M^w{}^*C_L^\circ}. \quad (21)$$

These theoretical equations predict that in either of the three mechanisms, the plot of $r_s$ and $1/\omega c_s$ against $\omega^{-1/2}$ should yield straight lines with a common slope, $\sigma$, which is defined by

$$\sigma = \frac{RT}{z^2F^2A}\cdot\frac{1}{^*C_L^\circ\sqrt{2D_L^\circ}}\cdot\frac{(1+\rho_c)^2}{\rho_c}. \quad (22)$$

The $\sigma$ value should be inversely proportional to $^*C_L^\circ$ but be independent of $^*C_M^w$. These predictions agreed with the experimental results shown in Figs. 5 and 6. Figure 7 shows the plot of $\sigma^*C_L^\circ$ against $E_{d.c.}$. The solid line in this figure is the theoretical line calculated by Eq. 22 using $D_L^\circ=2.3\times10^{-6}$ cm$^2$ s$^{-1}$. Thus the experimental dependence of $r_s$ and $1/\omega c_s$ on $\omega^{-1/2}$ can be explained equally well by any of the mechanisms EC, CE, or E. On the other hand, the theoretical Eqs. 14, 18, and 21 predict that in the EC mechanism $r_k$ ($\equiv(r_s-1/\omega c_s)$) should vary linearly with $(^*C_L^\circ)^{-1/2}$ (Eq. 14), whereas in the CE and E mechanisms $r_k$ should be inversely proportional to $^*C_L^\circ$ (Eqs. 18 and 21). In Figs. 8 and 9 $r_k$ obtained at $E_{d.c.}=E_{1/2}^r$ for the case of $^*C_M^w=0.1$ mol dm$^{-3}$ is plotted against $(^*C_L^\circ)^{-1/2}$ or $(^*C_L^\circ)^{-1}$, respectively. The plot of $r_k$ against $(^*C_L^\circ)^{-1/2}$ (Fig. 8) appears to be linear in the concentration range studied, but the intercept of the straight line at $(^*C_L^\circ)^{-1/2}=0$ was negative. This is inconsistent with the theoretical equation 14 (EC mechanism), which predicts a positive (or zero) intercept. Also, Eq. 14 predicts that the following inequality should hold in the EC mechanism:

$$(r_s - 1/\omega c_s) > \frac{RT}{z^2F^2A}\cdot\frac{K^\circ}{\rho_c}\left(\frac{1+\rho_c}{k_1^f D_L^\circ{}^*C_L^\circ}\right)^{1/2}. \quad (23)$$

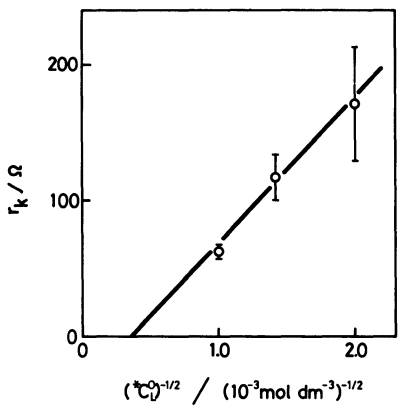


Fig. 8. Plot of $r_k(\equiv(r_s-1/\omega c))$ at $E_{d.c.}=E_{1/2}^r$ and $^*C_M^w=0.1$ mol dm$^{-3}$ against $(^*C_L^\circ)^{-1/2}$. The vertical bars indicate the standard deviations.

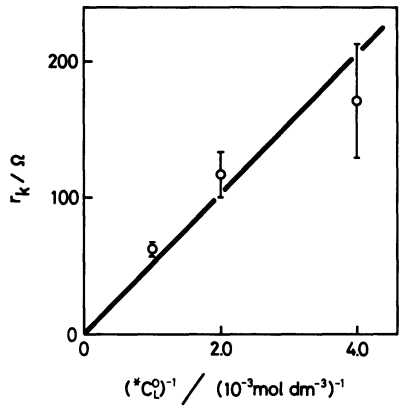


Fig. 9. Plot of $r_k(\equiv(r_s-1/\omega c_s))$ at $E_{d.c.}=E_{1/2}^r$ and $^*C_M^w=0.1$ mol dm$^{-3}$ against $(^*C_L^\circ)^{-1}$. The vertical bars indicate the standard deviations.

Application of this inequality to the result given in Fig. 5 with $K^\circ=9.8\times10^6$ mol$^{-1}$ dm$^3$ and $D_L^\circ=2.3\times10^{-6}$ cm$^2$ s$^{-1}$, as determined in this paper, yielded the lowest limit of $k_1^f$ to satisfy Eq. 14 as $k_1^f>1.5\times10^{13}$ mol$^{-1}$ dm$^3$ s$^{-1}$. This value seems unreasonably high for a bimolecular reaction in solution. According to Debye,[21] the rate constant for a diffusion-controlled bimolecular reaction, $k_D$, is given by

$$k_D = 4\pi N_L(D_A+D_B)r_D, \quad (24)$$

where $N_L$ is the Avogadro constant, $D_A$ and $D_B$ are the diffusion coefficients of the reactants A and B, and $r_D$ is the reaction distance. Using $r_D=1.5\times10^{-7}$ cm and $(D_A+D_B)=10^{-5}$ cm$^2$ s$^{-1}$, we obtain $k_D=1.1\times10^{10}$ mol$^{-1}$ dm$^3$ s$^{-1}$. These results indicate that the EC mechanism should be excluded from the present system. The plot shown in Fig. 9 indicates that $r_k$ is inversely proportional to $^*C_L^\circ$, suggesting that both the CE mechanism (Eq. 18) and the *E* mechanism (Eq. 21) are applicable to the present system. For the CE mechanism, the following inequality is predicted from Eq. 18:

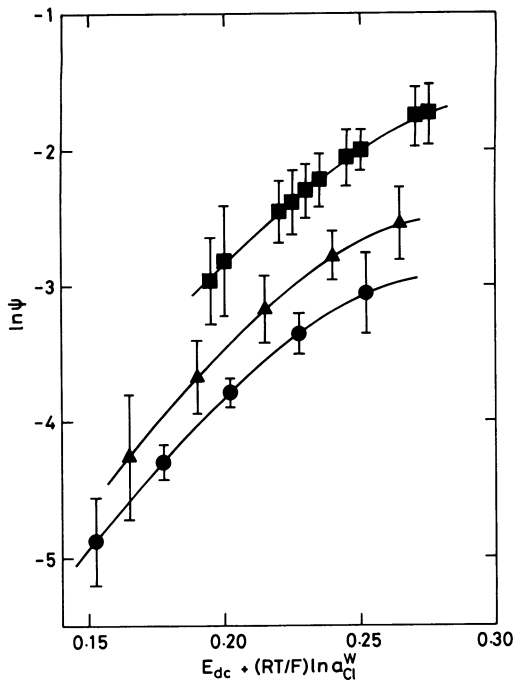


Fig. 10. Plot of $\ln\psi$ against $E_{d.c.}+(RT/F)\ln a^{W}_{Cl}$. $*C^{W}_{M}$: (■) 0.05; (▲) 0.1; (●) 0.2 mol dm$^{-3}$. The vertical bars indicate the standard deviations.

$$(r_s - 1/\omega c_s) > \frac{RT}{z^2F^2A}\cdot\frac{(1+\rho_c)d_L}{K^W *C^W_M *C^\circ_L}\left[\frac{K^W(K^W *C^W+1)}{k^f_2 D^W}\right]^{1/2}. \quad (25)$$

Application of this inequality to the results shown in Fig. 5 with $K^w$=14.6 mol$^{-1}$ dm$^3$,[19] $d_L$=2.3×10$^4$,[18] and $D^w$=10$^{-5}$ cm$^2$ s$^{-1}$ leads to the lowest limit of $k^f_2$ to satisfy Eq. 18 as $k^f_2$>2.7×10$^{12}$ mol$^{-1}$ dm$^3$ s$^{-1}$. When another value of $d_L$=2×10$^3$, which is calculated from the solubility data of DB18C6 in water[22] and nitrobenzene,[23] is used, we obtain $k^f_2$>2×10$^{10}$ mol$^{-1}$ dm$^3$ s$^{-1}$. Either value suggests a very low probability of the CE mechanism, which leads us to the conclusion that the E mechanism is the most probable mechanism for the present system.

In Fig. 10 the logarithm of $\psi$ defined by

$$\psi = \frac{RT}{z^2F^2A}\cdot\frac{(1+\rho_c)}{*C^W_M *C^\circ_L}\cdot\frac{1}{(r_s - 1/\omega C_s)} \quad (26)$$

is plotted against the corrected d.c. potential, $(E_{d.c.})_{corr}=E_{d.c.}+(RT/F)\ln a^{W}_{Cl}$ (see Results). In the E mechanism, $\psi$ can be given from Eq. 21 by

$$\psi = \vec{k}_{M/ML}(E_{d.c.}). \quad (27)$$

Figure 10 shows that the rate constant of the interface reaction of the E mechanism (Eq. 3) $\vec{k}_{M/ML}(E_{d.c.})$ depends on the potential difference across the nitrobenzene/water interface, $\Delta\phi$, and that $\vec{k}_{M/ML}(E_{d.c.})$ increases with increasing positive $\Delta\phi$. This seems quite reasonable. Figure 10 also shows that the rate constant at a given potential difference increases with decreasing NaCl concentration in the aqueous phase. This result indicates that the rate constant of the interface reaction is highly dependent on the structure of the electric double layer at the interface.[13,14]

Equation 18 implies that, if the CE mechanism would be applicable to the present system, the dependence of the $\psi$ values on the NaCl concentration ($*C^W_M$) could in part be explained by the second term in the square brackets on the right-hand side of Eq. 18. On the other hand, the dependence of $\psi$ on $\Delta\phi$ in Fig. 10 implies that the first term in the square brackets is not negligible, which in turn implies that the value of the bimolecular-reaction rate constant $k^f_2$ should be larger than a theoretically possible value of a bimolecular reaction in solution, as discussed above.

In conclusion, it can be stated that the a.c. polarographic behavior of the transfer of $Na^+$ ion facilitated by DB18C6 at the nitrobenzene/water interface is explained most reasonably by the interface reaction mechanism (E mechanism) of the three mechanisms that have been proposed.

## References

1) J. Koryta, *Electrochim. Acta*, **24**, 293 (1979).
2) A. Hofmanova, L. Q. Hung, and W. Khalil, *J. Electroanal. Chem. Interfacial Electrochem.*, **135**, 257 (1982).
3) Z. Samec, D. Homolka, and V. Mareček, *J. Electroanal. Chem. Interfacial Electrochem.*, **135**, 265 (1982).
4) D. Homolka, K. Holub, and V. Mareček, *J. Electroanal. Chem. Interfacial Electrochem.*, **138**, 29 (1982).
5) E. Makrlik, L. Q. Hung, and A. Hofmanova, *Electrochim. Acta*, **28**, 847 (1983).
6) P. Vanýsek, W. Ruth, and J. Koryta, *J. Electroanal. Chem. Interfacial Electrochem.*, **148**, 117 (1983).
7) E. Makrlik and L. Q. Hung, *J. Electroanal. Chem. Interfacial Electrochem.*, **158**, 277 (1983).
8) E. Makrlik, *J. Colloid Interface. Sci.*, **97**, 595 (1984).
9) J. Koryta, G. Du, W. Ruth, and P. Vanýsek, *Faraday Discuss. Chem. Soc.*, **77**, 209 (1984).
10) Wang Erkang and Pang Zhicheng, *J. Electroanal. Chem. Interfacial Electrochem.*, **189**, 21 (1985).
11) Z. Yoshida and H. Freiser, *J. Electroanal. Chem. Interfacial Electrochem.*, **179**, 31 (1984).
12) J. Koryta, *Ion-selective Electrode Rev.*, **5**, 146 (1983).
13) T. Osakai, T. Kakutani, and M. Senda, *Bull. Chem. Soc. Jpn.*, **57**, 370 (1984).
14) T. Osakai, T. Kakutani, and M. Senda, *Bull. Chem. Soc. Jpn.*, **58**, 2626 (1985).
15) The main results of the present paper were presented at the 30th Annual Meeting on Polarography and Electroanalytical Chemistry, Oct. 12—13, 1984, Hiroshima; Abstract, T. Kakutani, Y. Nishiwaki, T. Osakai, and M. Senda, *Rev. Polarogr. (Kyoto)*, **30**, 30 (1984).
16) T. Kakutani, T. Osakai, and M. Senda, *Bull. Chem. Soc. Jpn.*, **56**, 991 (1983).

17) J. Rais, *Collect. Czech. Chem. Commun.*, **36**, 3235 (1971).
18) T. Iwachido, M. Minami, A. Sadakane, and K. Toei, *Chem. Lett.*, **1977**, 1511.
19) E. Shchori, N. Nae, and J. Jagur-Grodzinsky, *J. Chem. Soc. Dalton Trans.*, **1975**, 2381.
20) The present authors, in preparation.
21) P. Debye, *Trans. Electrochem. Soc.*, **82**, 265 (1942).
22) C. J. Pedersen, *J. Am. Chem. Soc.*, **89**, 7017 (1967).
23) Y. Marcus and L. E. Asher, *J. Phys. Chem.*, **82**, 1246 (1978).
24) Lin Sinru and H. Freiser, *J. Electroanal. Chem. Interfacial Electrochem.*, **191**, 437 (1985).